Case C. Two tilts of equal magnitude in the same sense, i.e. $\alpha=\beta$

From (1)

$$\sin\theta = \sin^2\alpha + \cos^2\alpha \sin\theta_M , \quad (6)$$

and combining with equation (3),

$$\frac{\delta d}{d} = \sin^2\alpha \left(\frac{1-\sin\theta_M}{\sin\theta_M}\right). \quad (7)$$

Using the approximation for small α gives

$$\frac{\delta d}{d} = \alpha^2 \left(\frac{1-\sin\theta_M}{\sin\theta_M}\right). \quad (8)$$

$|\delta d/d|$ is to be subtracted from d_M in this case.

Case D. Two tilts of equal magnitude in opposite sense, i.e. $\alpha=-\beta$

Proceeding as before gives

$$\frac{\delta d}{d} = -\alpha^2 \left(\frac{1+\sin\theta_M}{\sin\theta_M}\right). \quad (9)$$

$|\delta d/d|$ is to be added to d_M.

Discussion

When only one tilt is involved the error in the value of d is independent of θ and, as Bond pointed out, such an error cannot be detected by making measurements of different orders of reflexion from the same plane. Equations (8) and (9) clearly show that Bond's assumption that the two errors are additive and thus also independent of θ is not correct. In terms of absolute errors such an assumption is also incorrect as the values of $\delta d/d$ for some particular values of α, β and θ show. These are given in Table 1.

When α and β are in the same sense the combined error is opposite in sign and smaller in magnitude than that due to either α or β alone, *i.e.* the errors due to specimen and beam tilt are partially compensating. At $\theta=90°$ compensation is perfect.

For opposite tilts the combined error is of the same sign but larger in magnitude than that computed by simple addition of the two errors considered to be independent. At $\theta=85°$, if the errors were independent, the total error for $\alpha=\beta=0{\cdot}001$ rad would be 10^{-6} compared with an actual error of 2×10^{-6}. Clearly when using this technique it is desirable to make α and β as small as possible, and as far as is possible to ensure that any residual tilts of beam and specimen are in the same direction.

References

BOND, W. L. (1960). *Acta Cryst.* **13**, 814.
D'HEURLE, F. M., FEDER, R. & NOWICK, A. S. (1963). *J. Phys. Soc. Japan*, **18**, Sup. II, 184.

Acta Cryst. (1968). A**24**, 685

Thermal Etching of (100) Surfaces in Sodium Chloride Single Crystals

BY G. TORRES V.
Centro de Investigación de Materiales, Universidad de México, México, D. F.

AND I. ALVAREZ E.* AND S. REYES L.†
Instituto de Física, Universidad de México, México, D. F.

(*Received* 6 *October* 1967 *and in revised form* 24 *May* 1968)

Freshly cleaved sodium chloride single crystals thermally etched both in air and in vacuum (10^{-5} torr) show three types of evaporation pit: concentric square pits and concentric circular pits in air etched crystals, and pyramidal pits in vacuum etched crystals. The pyramidal pits may be of three kinds: those with symmetric diagonals, those with one symmetric and one non-symmetric diagonal, and finally those with two non-symmetric diagonals. These pyramidal pits are of the same nature as those associated with dislocations, found on chemical etching of LiF crystals. The differences between pits produced in air and pits produced in vacuum are discussed in terms of surface fusion.

Introduction

When freshly-cleaved faces of sodium chloride single crystals are thermally etched (by heating them up to a temperature near the melting point), pits and other corrosion figures are produced due to the evaporation of the crystal. Grinberg (1963) reported that no relationship was found between the development of the pits and the structural crystal defects in sodium chloride single crystals, but that the pits are produced when the surface is changing to higher equilibrium states; however, a relationship between evaporation pits and crystal defects was shown by Patel, Bahl & Vagh (1965) for the case of sodium chloride.

* Fellow of the Comisión Nacional de Energía Nuclear and the Instituto Nacional de la Investigación Científica, México, D. F.
† Facultad de Ciencias, Universidad de México, México, D. F.

In the present work, a study has been made of the behaviour of sodium chloride single crystals under different conditions of temperature and atmosphere.

Experimental method and results

Crystals were grown by a modified Kyropoulos method as described by Fernández & Muñoz (1962). The samples were cleaved from the crystals and thermally etched in a tubular furnace. The surfaces were examined under an optical microscope and in an electron microscope using carbon-gold replica techniques.

The samples were etched both in air and in vacuum under the following conditions:

(1) Constant time intervals and variable temperature.
(2) Variable time intervals and different fixed temperatures.

Other samples were weakly thermally etched in air to observe the initial evaporation at electron microscope level.

Thermal etching in air

The first visible effects of thermal etching in air, for a surface held in the furnace for $1\frac{1}{2}$ hours, appear at 640 °C. On the surface, two evaporation figures are observed: pits formed by concentric and non-concentric squares, the density of which is low (10^2 per cm^2); and steps, which we call evaporation fronts (Fig. 1). The movement of the evaporation fronts is a result of the evaporation of kinks, as was shown by Wainer & Abeledo (1965).

At 700 °C after $1\frac{1}{2}$ hours, circular pits appear and these are of two types formed by concentric and by non-concentric circles, Fig. 2. The pits retain the circular shape even at temperatures very near the melting point.

After 2 hours at 640 °C, the samples show interactions between pits, but even after 72 hours in the furnace the square shape of the pits is conserved. As the pits grow, their edges form new evaporation fronts, and their effects are added to the fronts growing from the crystal edges. The net result is that pits slowly disappear. If the temperature is increased, but is still less than 680 °C, the etching stages develop faster; that is, the crystal is more rapidly crossed by the evaporation fronts, implying a more intensive evaporation. When crystals are thermally etched at 700 °C, pits appear in times as short as 20 minutes; these pits are circular. After 6 to 8 hours at this temperature the pits interfere with, and finally annihilate, one-another. If the temperature is increased each stage appears sooner. The results are summarized in Table 1.

Thermal etching in vacuum

In crystals thermally etched in vacuum, after 30 minutes at 620 °C, square pits appear which are point-bottomed, and lie parallel to the directions of the *a* axes. The density of these pits is 10^2 per cm^2. Crystals maintained at 680 °C for 15 minutes show a high density of pyramidal pits (Fig. 3). The fact that some of the pits are point-bottomed and others flat-bottomed indicates a movement, or removal, of the pit origin. At higher temperatures, in vacuum, there is no change in the pattern, the process being only accelerated, and the pits appearing more rapidly. Fig. 4 shows a strongly vacuum-etched surface (1 hour at 725 °C). The appearance of new pits inside the former ones can be observed, as well as the extremely shallow depth of the

Table 1. *Thermal etching in air*

Time (hr)	Temperature (°C)	Density (pits/cm^2)	Evaporation pattern
1·5	640–680	10^2	Concentric and non-concentric square pits. At this temperature non-etching pattern appears before this etching time.
1·5	700 to melting point	High (10^3–10^4)	Concentric and non-concentric circular pits.
2·0	640		Square pits interacting with one another.
2·0–72·0	640–680		Square shape is conserved. New evaporation fronts are formed adding their effects to the fronts growing from the crystal edges. The net result is that pits slowly disappear.
10–15 minutes	700	High	Circular pits. Circular shape is obtained from the beginning. Observable with electron microscope.
6·0–8·0	700	High	Circular pits. Pits interfere with, and annihilate, one-another.
1·0–72·0	700 to melting point	High	Circular pits. Stages appear faster.

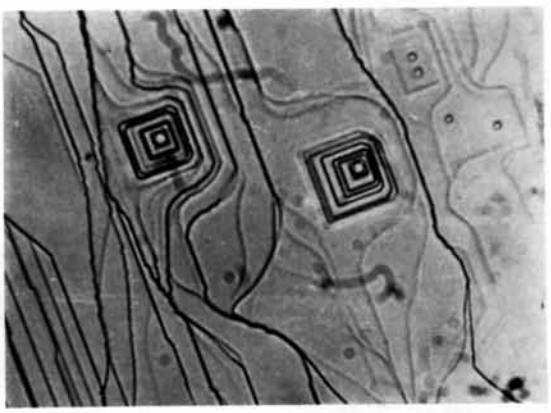

Fig. 1. Pits formed by concentric and non-concentric squares, produced in air after 1½ hours at 640°C. Note the large density of evaporation fronts on the surface (×225).

Fig. 2. Circular pits developed at 700°C in air. Etching time of 1½ hours (×225).

Fig. 3. Point-bottomed pyramidal pits developed in vacuum after 30 minutes at 680°C (×225).

[*To face p.* 686

Fig. 4. Example of a strongly thermally etched crystal. 1 hour in vacuum at 725 °C (× 225).

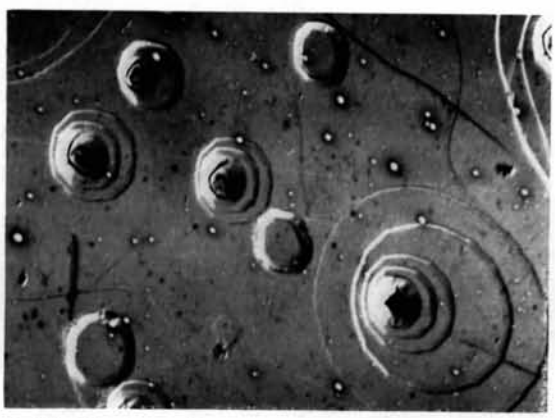

Fig. 6. Weakly thermally etched crystal. 10 minutes at 700 °C in air. Note that the pits are approximately circular from the beginning (× 32,000).

evaporation fronts, undetectable by an optical microscope.

In crystals etched in vacuum it is possible to distinguish three kinds of pyramidal pit (Fig. 5): with symmetric diagonals, with one symmetric and one non-symmetric diagonal, and with two non-symmetric diagonals. These pyramidal pits are of the same type as those associated with dislocations, found by Gilman, Johnston & Sears (1958) on chemical etching of LiF crystals, and by Mendelson (1961) in sodium chloride single crystals. The results are summarized in Table 2.

Surfaces weakly etched in air

In order to study the origin of the pits, a special etching technique was used for the observation of the initial stages of evaporation. Surfaces were etched in air for very short times (10 minutes at 700 °C) and observations were then made in an electron microscope using the carbon-gold replica technique.

The results are shown in Fig. 6. It was observed that the pits were approximately circular from the very beginning so they are probably not the result of the evolution of square pits, as Grinberg (1963) proposed. The pits have a definite origin and may be associated with an imperfection in the crystal. We refer to Patel, Bahl & Vagh (1965) who have shown the relationship between evaporation pits and linear imperfections.

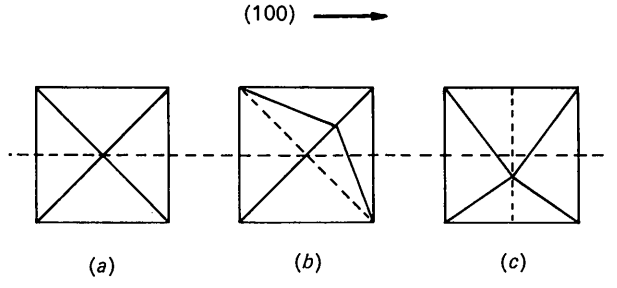

Fig. 5. Different kinds of pit. (*a*) Symmetric diagonals. (*b*) One symmetric and one non-symmetric diagonal. (*c*) Two non-symmetric diagonals.

Thermal etching in nitrogen and oxygen atmospheres

An attempt was made to determine the influence of the furnace atmosphere on the evaporation fronts. Some crystals were thermally etched at 700 °C in nitrogen or oxygen atmospheres for one hour. In both atmospheres the appearance of circular pits was observed. We can conclude that neither the nitrogen nor the oxygen has an influence on the pit shape. However, the rate of evaporation in the oxygen atmosphere was higher than in nitrogen. This may be due to an adsorption of oxygen by the surface, in such a way that the surface energy is lowered.

Summary and conclusions

In air at temperatures between 640 °C and 680 °C square pits develop and maintain that shape even for etching times of 70 hours. Above 690 °C circular pits appear. In vacuum there is a complete absence of circular pits, *i.e.* thermal etching in vacuum produces only square pits.

The evaporation of the surface proceeds through evaporation fronts, which originate at the crystal edges and at preferential points. In crystals etched in air, the evaporation fronts are so thick that they are visible in an optical microscope. As Patel, Bahl & Vagh (1965) showed, these preferential points occur where dislocation lines intersect the cleavage surface. There is no obvious explanation for the three kinds of pit, two of which are formed in air (Figs. 1 and 2), and one in vacuum (Fig. 3.) However, the following could be the explanation: at temperatures higher than 680 °C the surface starts to melt, forming a thin liquid layer. As the material starts to evaporate at low energy sites, such as defects, an evaporation pit of circular shape is originated (Fig. 6), whose circular shape will be preserved by surface tension forces. The pit will increase its size until the defect at the origin disappears.

Far from the source, the speed of the evaporation fronts will be decreased (by impurities, temperature

Table 2. *Thermal etching in vacuum*

Time (min)	Temperature (°C)	Density (pits/cm²)	Evaporation pattern
30	620	10^2	Pyramidal pits. Square pits point-bottomed.
15–60	680	High	Pyramidal pits, point- and flat-bottomed. The appearance of such pits indicates a movement or removal of their origin.
15	680 to melting point		No change in the pattern, process being only accelerated. Pits appear more rapidly.
60	725		Square pits. New pits appear inside the originals.
15	Very near melting point		Square pits.

gradients, *etc.*) and the interaction between them will produce an increment in the thickness of the front. The evaporation front then becomes visible. Note for example that in Fig. 6 the thickness is 0·3 micron and in Fig. 2 it is up to 1 micron.

In vacuum, the process is carried out in a different way. The low pressure (10^{-5} torr) does not allow the formation of the melt layer on the surface and, thus, the material goes directly from the solid to the vapor phase. The net result is that circular pits are not developed.

It is a pleasure to record the helpful and stimulating discussions with Professor N. Cabrera and H. Riveros, as well as the help of A. Valladares and J. A. Careaga in the preparation of the manuscript.

References

FERNÁNDEZ, A. & MUÑOZ, E. (1962). *Rev. Mex. Fís.* XI, 255.
GILMAN, J. J., JOHNSTON, W. G. & SEARS, G. W. (1958). *J. Appl. Phys.* **29**, 747.
GRINBERG, A. (1963). *Phys. Stat. Sol.* **3**, 1369.
MENDELSON, S. (1961). *J. Appl. Phys.* **32**, 1579.
PATEL, A. R., BAHL, O. P. VAGH, A. S. (1965). *Acta Cryst.* **19**, 1025.
WAINER, L. S. DE & ABELEDO, M. J. DE (1965). *Brit. J. Appl. Phys.* **16**, 1764.

Acta Cryst. (1968). A**24**, 688

Diffuse Diffraction Phenomena from Neutron-Irradiated Graphite Single Crystals

BY W. T. EELES†

Berkeley Nuclear Laboratories, Berkeley, Gloucestershire, England

(*Received* 4 *April* 1968)

Single crystals of neutron irradiated graphite have been found to show diffuse diffracted intensity in the form of rel-rods through the *hki*0 reflexions and parallel to **c***. Off-axis broadening of the 000*l* reflexions has also been observed.

Powder diffraction studies of irradiated graphite (Bacon & Warren, 1956; Eeles, 1962) have shown that radiation damage in graphite results in peak shifts, line broadening and changes in small-angle scattering. These observations are consistent with measurements of other physical properties such as bulk growth and stored energy, and lead to a picture of damage in graphite irradiated at low temperatures (< 300 °C) in which displaced carbon atoms are distributed at random, singly or in small clusters, between the layer planes. The layer structure is thus distorted primarily in the **c** direction. The author has taken oscillation photographs of small single crystals of Ticonderoga graphite irradiated with neutrons to a dose of 2×10^{20} n.v.t. (Ni) at a temperature of 200 °C.

Figs. 1, 2 and 3 are oscillation photographs of the irradiated crystals, while Figs. 4 and 5 are oscillation photographs of unirradiated crystals of comparable size, taken under identical conditions to those of Figs. 1 and 2. Comparison of Figs. 1 and 4 shows that neutron irradiation has caused extensive asymmetric axial broadening of the 000*l* reflexions. These reflexions are also diffuse in directions at right angles to **c***. That may simply be because of macroscopic mis-orientated regions which often occur in Ticonderoga graphite, or it may be spreading of the reflexions in reciprocal space. The 0002 reflexion is in fact so diffuse that it appears in photographs taken with **c** as axis of oscillation (Fig. 2).

Fig. 2 shows another striking feature when compared with Fig. 5, *viz.* continuous rods of diffuse intensity on the row lines passing through each *hki*0 reflexion. The rods are shown in cross-section in Fig. 3, which is a stationary crystal photograph taken with **c** parallel to the incident X-ray beam. **c**-Axis strain could cause extension of the *hkil* reflexions but it cannot give rise to the diffuse intensity around the *hki*0 reflexions since the reciprocal lattice vectors for these reflexions are at right angles to the strain. **a**-Axis strains would broaden these reflexions along the *hki*0 reciprocal lattice vectors, not at right angles to them as in the present case.

Factors which are known to extend the *hki*0 reflexions parallel to **c*** are (Wilson, 1949) stacking faults in which adjacent layers are displaced relative to one another by $\frac{1}{3}[11\bar{2}0]$, and twist boundaries (turbostratic disorder) in which adjacent layers are rotated with respect to one another about the **c** axis by random amounts. The first kind of fault would not affect $11\bar{2}0$ reflexions at all, while the second kind would give diffuse intensity as cylinders with **c*** as axis, rather than rods (*cf.* Fig. 3). A third type of fault, translation of layers by random amounts in the $[11\bar{2}0]$ direction, is consistent with rods passing through all *hki*0 reflexions

† Present address: Electricity Council Research Centre, Capenhurst, Chester, England.